Short-ranged ordering for improved mean-field simulation of disordered media: insights from refractory-metal high-entropy alloy carbonitrides

Okan K. Orhan,^{1,2} Mewael Isiet,² Mauricio Ponga,^{2,*} and David D. O'Regan¹

School of Physics, SFI AMBER Centre, and CRANN Institute,

Trinity College Dublin, the University of Dublin, Ireland

Department of Mechanical Engineering, the University of British Columbia,

2054 - 6250 Applied Science Lane, Vancouver, BC, V6T 1Z4, Canada

Multi-principal element materials (MPEMs) have been attracting a rapidly growing interest due to their exceptional performance under extreme conditions, from cryogenic conditions to extremehigh temperatures and pressures. Despite the simple conceptual premise behind their formation, computational high-throughput first-principles design of such materials is extremely challenging due to the large number of realizations required for sufficient statistical sampling of their design space. Furthermore, MPEMs are also known to develop short-ranged orderings (SROs) which can play a significant role in their stability and properties. Here, we present an expedient and efficient first-principles computational framework for assessing the compositional and mechanical properties of MPEMs, including SRO effects. This heuristic methodology systematically corrects phase-averaged free-energies of MPEMs to include SRO phases, while imposing constraints for materials design. To illustrate the methodology, we study the stability and mechanical properties of equi-molar refractory-metal high-entropy alloy carbonitrides (RHEA-CNs) such as ZrNbMoHfTaWC₃N₃. We show that SRO, arising due to preferential neighboring among refractory metals, is necessary for thermodynamic and mechanical stability and to satisfy the imposed design criteria, leading to complex compositions for which their molar fraction and mechanical properties are predicted.

High-entropy materials (HEMs) such as high-entropy alloys [1-3], oxides [4, 5], and high-entropy ceramics [6, 7] are mostly equi-molar multi-principal element materials (MPEMs), not exhibiting any long-ranged configurational ordering. They are known for their exceptional thermodynamic stability [8], hardness and strength [9-14], wear resistance [15-17], and oxidation resistance [15, 18]. As the refractory metals and their conventional alloys are already well-known for their high melting points, corrosion resistance, and high strength at high temperature [19], the refractory high-entropy allovs (RHEAs) [20–22] are naturally promising candidates materials for tailored properties under extreme environments [23, 24]. However, they often have poor ductility, high-density and poor oxidation resistance [25, 26]. Engineering the RHEA ceramics such as RHEA carbides [24, 27, 28], or nitrites [29, 30] with improved durability have attracted considerable interest as alternatives to Ni-based super-alloy carbides/nitrites, which are the industry standard materials choice for high temperature and high stress device components [31, 32].

The early conceptual definition of HEMs was that the high configurational entropy (S_{conf}) leads to thermodynamic stabilization by lowering the mixing Gibbs free energy (GFE) due to a full configurational randomness [1–3]. Although this over-simplified definition serves as a valuable preliminary criterion, it has been shown that the mechanisms behind their formation are far more complex [33]. In particular, the short-ranged orderings (SRO) play a significant role in determining materials properties due to local lattice distortion and complex local chemical environments [33–36]. This significantly hin-

ders first-principles simulations for high-throughput materials design as a large number of quasi-random supercells are necessary for proper statistical representation of the design space. The high computational cost of first-principles simulations combined with the large number of configurational representations needed make the exploration of the compositional space restricted, ultimately hampering novel materials discovery. In order to push the boundaries of MPEMs design and to capture a wide spectrum of materials properties, hybrid computational approaches beyond conventional first-principles methods are required [37].

In this letter, we present a computationally expedient corrective approach method to introduce SRO to MPEMs at the disordered mean-field limit. Using a prescribed subset of possible local crystal structures of their principal elements, combined with multi-objective optimization, local compositions and molar fractions due to SRO are determined. The newly developed approach is demonstrated on the equi-molar RHEA carbonitrides (RHEA-CN). While we focus in the RHEA-CNs, this methodology can be easily extended to any other MPEMs both with single or multiple phases.

A RHEA-CN is described as five or six of zirconium (Zr), niobium (Nb), molybdenum (Mo), hafnium (Hf), tantalum (Ta) and/or tungsten (W)) randomly occupying metallic sites of the rock-salt structure (B32), while C or N occupy the interstitial sites at same proportions, as shown in Fig. 1. To make notation short, we label compositions using X_j^m , for which m is the number of the distinctive metals and j serves to distinguish every possible equi-molar mixture. Similarly, the equi-molar mixture of

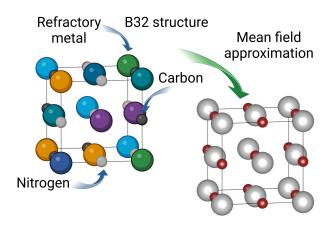


FIG. 1. The representative conventional unit cell of the rocksalt structure, also called B32. On the left, a realization of RHEA-CN with refractory metal ions denoted with larger spheres. On the right, a mean field approximation using virtual atoms. The metallic and interstitial sites are shown with gray and red, respectively.

C and N is labeled by Y^2 . By way of example, $X_1^6Y^2$ represents the equi-molar mixture of ZrNbMoHfTaWC₃N₃ while $X_1^5Y^2$ represents $Zr_2Nb_2Mo_2Hf_2Ta_2C_5N_5$. The full list of the simulated equi-molar refractory-metal carbonitrides (R-CNs), which serves as the database for the multi-objective optimization, can be found in the Supplementary Material (SM) [38].

The central quantity is the mixing Gibbs free energy (GFE), which is the almost-ubiquitous criterion to asses thermodynamic stability, given by [39]

$$G_{\text{mix}} = G_{\text{MPEM}} - \sum_{i}^{N} \alpha_i G_i. \tag{1}$$

Here, G_{MPEM} is the GFE of MPEM and G_i is the GFE of the i^{th} constituent with a molar fraction of α_i . In this work, the B32 structures of refractory-metal carbides (RCs) and nitrites (RNs) serve as the constituents, thus N=2M where M is the number of the distinct refractory-metals and $\alpha_i=1/N$. G_{MPEM} is approximated by

$$G_{\text{MPEM}} = G_{\text{RSS}} + G_{\text{SRO}},\tag{2}$$

where $G_{\rm RSS}$ is the GFE of the random-solid solution (RSS) and $G_{\rm SRO}$ is a SRO correction, given by

$$G_{\text{SRO}} = \sum_{m=1}^{M-1} \sum_{i}^{\binom{M}{m}} \beta_j^m \left(\Delta G_j^m + \Delta U_j^m \right), \tag{3}$$

where β_j^m are the *optimal* molar fractions of the subsystems. The compound-index (m, j) represents a subsystem in the database, corresponding to m of the M principal elements and numbered by j (see SM [38]).

The first term in Eq. (3) is simply the GFE difference between the (m,j) sub-system and the RSS, given by $\Delta G_j^m = \left[G_j^m - G_{\rm RSS}\right]$. The second term in Eq. (3), ΔU_j^m , is the elastic potential energy contribution due to the elastic mismatch between the (m,j) sub-system and the RSS, which can be interpreted as the strain energy stored in an inclusion inside an elastic matrix [40]. Since the clustering of the sub-systems is unknown a priori, we estimate this term for compatible crystal structures as $\Delta U_j^m = K_j^m \Delta V_j^m$, where K_j^m is the bulk modulus of the (m,j) sub-system and the absolute volume difference is given by $\Delta V_j^m = |V_j^m - V_{\rm RSS}|$. More sophisticated continuum theories can be used to predict shape and volume of these sub-systems if interface energies are also accounted [41].

Minimizing the G_{mix} via adjustment of the atomic molar fractions (β_j^m) of the SRO phases, becomes the primarily objective to ensure thermodynamic stability of the MPEM. In the present work, we also explore a further refinement of this objective. It has been shown that three simple solubility indicators play significant roles in formation of MPEMs [42, 43]. The first one is the lattice mismatch parameter, given by

$$\delta a = \sqrt{\sum_{m=1}^{M-1} \sum_{j}^{\binom{M}{m}} \beta_j^m \left(1 - \frac{a_j^m}{a_{RSS}}\right)^2},$$
 (4)

where a is the lattice parameter. The second solubility indicator is the valence-density mismatch parameter, given by

$$\delta n = \sqrt{\sum_{m=1}^{M-1} \sum_{j}^{\binom{M}{m}} \beta_{j}^{m} \left(1 - \frac{n_{j}^{m}}{n_{\text{RSS}}}\right)^{2}},$$
 (5)

where n is the valence-electron density per unit volume. The last indicator is the electronegativity mismatch parameter, given by

$$\delta \chi = \sqrt{\sum_{m=1}^{M-1} \sum_{j}^{\binom{M}{m}} \beta_j^m \left(1 - \frac{\chi_j^m}{\chi_{RSS}},\right)^2}$$
 (6)

where χ is the Mulliken electronegativity. Finally, two constraints, given by $\beta_m^j \leq \frac{1}{mM}$ and $\sum_{m=1}^{M-1} \sum_j^{\binom{M}{m}} \beta_j^m \leq 1$, are imposed to avoid double-counting. The former ensures that the total molar fractions of sub-systems with m principal elements is equal or less than 1, while the latter ensures that the total molar fractions of all subsystems are equal or less than 1.

In this work, we used multi-objective metaheuristics to optimize the molar fractions β_j^m Multi-objective metaheuristics [44] has been used in different aspects of materials design such as materials selection and design [45,

46], phase-stability prediction [47], and composition-dependent materials properties [37]. Specifically, we used the particle-swarm optimization (PSO) [48, 49], which is a stochastic multi-objective metaheuristics method, as it provides us a tractable approach for global optimal solution without requiring any initial guess or gradient information [50]. Thus, it is highly suitable for diverse set of problems especially when limited data sets are available for finding the optimal configurations [51–54] . It performs particularly well to build effective relationship without requiring an extensive data set [55]. We have made our code for optimizing the β_j^m freely available for use at Ref. 56.

Our framework is suitable to be used with any materials database which provides the GFE, a, n and χ of the RSS of MPEM and its sub-systems. In this work, the approximate Kohn-Sham density-functional theory (KS-DFT) [57–59] is used with the virtual-crystal approximation (VCA) [60, 61] to statistically represent random-solid solutions at the disordered mean-field limit. The VCA is practically applied through a linear mixing scheme of the atomic pseudopotentials within the practical KS-DFT [61]. Virtual atoms with the weightedaverage electron count and the corresponding weightedaverage potential of the parent elements were generated. Despite being oversimplified, it has been shown to be relatively accurate in calculating simple-phase transformation, thermodynamic functions, elastic constants, and tensile and shear strength of HEMs [62–66]. Thus, it is highly suitable to expediently obtain the GFE, crystallographic and elastic properties, and the Mulliken electronegativity, which is in practice approximated as the negative of chemical potential within KS-DFT [67].

An initial validation of the methodology can be gained by noting that, in Table S3 in SM [38], the calculated macroscopic Vickers hardness ($H_{\rm V}$) of RCs and RNs are in good agreement with the available experimental measurements, particularly considering that the experimental $H_{\rm V}$ highly depends on morphology and microstructure, direction of loading forces relative to crystallographic orientation, and impurities [68, 69]. Thus, despite its simplifications, the calculated $H_{\rm V}$ computed within the VCA can still serve as a figure of merit (FoM) for material hardness. We refer the reader to SM [38] for further details on methodology and computational details.

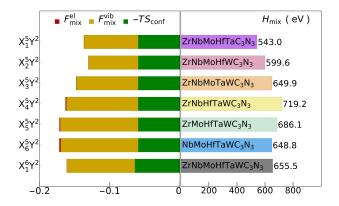


FIG. 2. The components of the mixing Gibbs free energy of the random-solid solutions of the refractory-metal high-entropy alloy carbonitrides the electronic at T=300 K. Here, $H_{\rm mix}$ and $S_{\rm conf}$ are the enthalpy of mixing and the configurational entropy, respectively, and $F_{\rm mix}^{\rm el}$ and $F_{\rm mix}^{\rm vib}$ are the electronic and vibrational Helmholtz free energies, respectively.

We commence our analysis by investigating the the components of $G_{\rm mix}$ of the RSSs when SRO effects are not considered for the X⁵ and X⁶ systems, portrayed in Fig. 2. The enthalpy of mixing $(H_{\rm mix})$ is the dominating contribution, pushing $G_{\rm mix}$ to large positive values compromising thermodynamic stability of RHEA-CNs. Among the remaining components, the mixing electronic Helmholtz free energy $(F_{\rm mix}^{\rm el})$ is mostly negligible while the vibrational Helmholtz free energy $(F_{\rm mix}^{\rm vib})$ and the configurational entropic contribution $(-TS_{\rm conf})$ at 300 K have still small, yet comparable contributions. Once again noting that SRO effects are still neglected, the observed trend under that approximation indicates that it may not be feasible to achieve a full configurational disorderliness.

The majority of the RSSs are nonetheless elastically stable according to the Born-Huang-stability criteria [70, 71](see SM [38] for further details) as listed in Table S2. However, if no SRO effects are considered, RHEA-CNs X_4^5 , X_5^5 and X_6^5 compositions are among the ones which fail to satisfy the Born-Huang stability criteria. The complex-valued phonon modes as indicated by the negative phonon density of states (shown in Fig. S3 in SM [38]), indicate that the isolated and strain-free RSSs of RHEA-CNs are not dynamically stable except the cases of X_1^5 and X_2^5 . Positive phonon frequencies without softer phonon modes indicate significantly lower possibility of phase transformation to lower symmetries at finite temperatures [72].

Furthermore, using semi-empirical relations, the mechanical performance of MPEMs can be also assessed. The Vickers hardness [73, 74], Poisson's ratio [75], and the Pugh ratio [76] are commonly used as FoMs to assess hardness, brittleness, and ductility, respectively. The calculated $H_{\rm V}$ of the mechanically stable RHEA-CN (listed in Table S4 in SM [38]) indicate that the full RSSs (no SRO effects) are not particularly promising in terms of

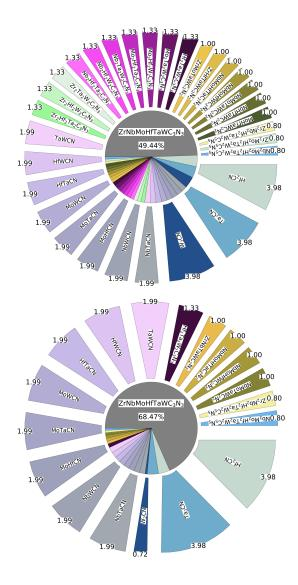


FIG. 3. The optimized short-ranged ordering correction parameters for $X_1^6Y^2$ (ZrNbMoHfTaWC₃N₃) using the single-objective (SO) (top) and the multi-objective (MO) (bottom) at 300 K). See **SM** [38] for the color codes.

mechanical hardness.

Having analyzed the RSS cases, we now proceed to include SRO effects and design criteria using the proposed framework. Two sets of SRO-correction parameters (β_j^m) were optimized for each equi-molar RHEA-CN. The first set was optimized using minimization of G_{SRO} as a single-objective (SO); the second set was optimized using a multi-objective (MO) technique including minimization of G_{SRO} subjected to Eqs. (4)-(6). The results are shown in Fig. 3 for ZrNbMoHfTaWC₃N₃ (X₁⁶Y²) at 300 K (see Figs. S4-S10 in SM [38] for the optimized β_j^m and PSO convergence behavior for other systems). We also refer the reader to Ref. 56 for the external database, used in the PSO, and the complete numerical results of

PSO for each system.

A general emerging trend is that the set of alloys for which there is a non-zero MO- β_j^m is a subset of the set SO- β_j^m . This observation indicates that G_{SRO} is the predominant objective; however, the solubility objectives (Eqs. (4)-(6)) are responsible for determining the allowed SRO phases and content. G_{SRO} also reaches convergence quicker for SO compared to that of their MO counterpoints.

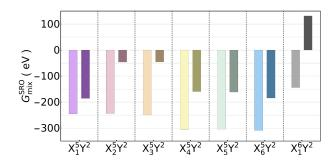


FIG. 4. The short-ranged ordering corrected mixing Gibbs free energy $(G_{\text{mix}}^{\text{SRO}})$ of the refractory-metal high-entropy alloy carbonitrides T=300~K using the single-objective (SO) (left lighter colors) and multi-objective (MO) (right darker colors) optimized short-ranged ordering parameters (β_i^m) .

In Fig. 4, the SRO-corrected $G_{\rm mix}$, namely $G_{\rm mix}^{\rm SRO}$, is shown for the both optimized sets of β_j^m (also listed in Table S5 in SM [38]). The SO- β_j^m leads to lower energies compared to their MO- β_j^m counterparts. This is due to the additional solubility FoMs, imposed as objectives, reducing the molar fraction of $G_{\rm SRO}$ phases. For the sake of simplicity, the relative weights of the four objectives are set to be equal during optimization. For the five refractory-metals RHEA-CNs, the SRO enables thermodynamic stability while also maintaining the solubility criteria. In the case of $X_1^6Y^2$, the SRO are not sufficient to thermodynamically stabilize it when the solubility FoMs are simultaneously imposed.

The SRO correction can be expediently carried to the elastic constants by

$$\mathbb{C}_{SRO} = \mathbb{C}_{VCA} + \sum_{m=2}^{M-1} \sum_{j}^{\binom{M}{m}} \beta_{j}^{m} \Delta \mathbb{C}_{j}^{m}, \tag{7}$$

where $\Delta \mathbb{C}_{j}^{m} = \left[\mathbb{C}_{j}^{m} - \mathbb{C}_{\text{VCA}}\right]$ and \mathbb{C} is the second-order elastic tensor. This leads to mechanical stabilization of X_{4}^{5} , X_{5}^{5} and X_{6}^{5} , which we have shown to fail the Born-Huang stability criteria without the SRO correction. Eq. (7) also improves mechanical properties, calculated using the aforementioned rule of mixing, listed in Table I. SO leads to higher bulk moduli compared to MO, as much as 43% higher in the case of $X_{1}^{6}Y^{2}$. This trend does not necessarily extend to the case for hardness as MO leads to higher H_{V} values (e.g., 5-10 GPa)

in the case of $X_1^5Y^2$ and $X_2^5Y^2$ since it also depends on the shear modulus (S). Nevertheless, the SRO-corrected H_V values are significantly higher compared to their RSS counterparts. Although H_V are smaller compared to the single-refractory-metal carbides or nitrites (listed in Table S3 in SM [38]), they still exhibit significant hardness. We furthermore also predict that they exhibit significant strength and workability due to their high Poisson's ratio and the Pugh ratio over the critical minimum values of 0.25 [75] and 1.75 [76], respectively.

	K		H	V	ν	'P	K/S	
	SO	МО	SO	МО	SO	МО	SO	МО
$X_1^5Y^2$	168	167	6.85	7.01	0.35	0.34	2.89	2.82
$X_2^5Y^2$	179	161	5.21	6.26	0.38	0.35	3.74	3.24
$X_3^5Y^2$	194	158	5.95	5.59	0.37	0.36	3.57	3.24
$X_4^5Y^2$	242	185	10.13	8.98	0.34	0.32	2.75	2.50
$X_5^5Y^2$	240	190	9.73	8.79	0.34	0.33	2.82	2.59
$X_6^5Y^2$	240	195	9.57	9.08	0.34	0.33	2.85	2.57
$X_1^6 Y^2$	183	128	7.83	7.50	0.34	0.31	2.77	2.25

TABLE I. The calculated bulk (K) and shear (S) moduli, and Vickers hardness $(H_{\rm V})$ (in GPa units), Poisson's ratio $(\nu_{\rm P})$ and the Pugh ratio (K/S) of the refractory-metal highentropy alloy carbonitrides using the single-objective (SO) and multi-objective (MO) optimized short-ranged ordering parameters (β_j^m) .

In this Letter, we demonstrated the effects of SRO on stability and mechanical properties of RHEA-CN. Despite the particular focus on these promising ceramics, our newly developed method offers a feasible approach to include SRO to the disordered mean-field limit. It is highly suitable to be used with any given external materials database as well as the carefully generated smaller in-house materials database of this exploratory investigation. Our implementation is also highly generalizable to introduce any additional objectives and/or constraints, specially selected for any materials class. Using our newly developed method, it was shown that SROs play crucial roles in thermodynamically and mechanically stabilizing RHEA-CNs. It was also shown that the single objective of minimizing the mixing GFE admits more diverse SROs, while the solubility objectives reduce the number of allowed SRO. However, in the more limiting case of imposing multi-objective optimization, SRO effects are not sufficient to achieve stability for the X_1^6 system. SRO correction leads to predicted mechanical strength and hardness to the traditional refractory carbides and nitrides, and points to better workability. These finding suggest that RHEA-CN materials can be appealing systems potentially with novel material properties. This investigation overall reveals the essential role of SRO effects, while opening up a practical route for their inclusion in high-throughput first-principles methods, and possibly in future the direct design of MPEMs for desired mechanical property combinations.

We acknowledge the support of Trinity College Dublin School of Physics, of Science Foundation Ireland (SFI) through The Advanced Materials and Bioengineering Research Centre (AMBER, grant 12/RC/2278 and 12/RC/2278.P2), and of the European Regional Development Fund (ERDF). We acknowledge the support from the from the Natural Sciences and Engineering Research Council of Canada (NSERC) through the Discovery Grant under Award Application Number RGPIN-2016-06114, and the New Frontiers in Research Fund (NFRFE-2019-01095). This research was supported in part through computational resources and services provided by Trinity Centre for High Performance Computing and Advanced Research Computing at the University of British Columbia.

- * Corresponding author: mponga@mech.ubc.ca
- [1] J.-W. Yeh, S.-K. Chen, S.-J. Lin, J.-Y. Gan, T.-S. Chin, T.-T. Shun, C.-H. Tsau, and S.-Y. Chang, Nanostructured high-entropy alloys with multiple principal elements: Novel alloy design concepts and outcomes, Advanced Engineering Materials 6, 299 (2004).
- [2] B. Cantor, I. Chang, P. Knight, and A. Vincent, Microstructural development in equiatomic multicomponent alloys, Materials Science and Engineering: A 375-377, 213 (2004).
- [3] J. W. Yeh, Recent progress in high-entropy alloys, Annales de Chimie. Science des Materiaux 31, 633 (2006).
- [4] C. M. Rost, E. Sachet, T. Borman, A. Moballegh, E. C. Dickey, D. Hou, J. L. Jones, S. Curtarolo, and J.-P. Maria, Entropy-stabilized oxides, Nature Communications 6, 8485 (2015).
- [5] A. Sarkar, L. Velasco, D. Wang, Q. Wang, G. Talasila, L. de Biasi, C. Kübel, T. Brezesinski, S. S. Bhattacharya, H. Hahn, and B. Breitung, High entropy oxides for reversible energy storage, Nature Communications 9, 3400 (2018).
- [6] J. Gild, Y. Zhang, T. Harrington, S. Jiang, T. Hu, M. C. Quinn, W. M. Mellor, N. Zhou, K. Vecchio, and J. Luo, High-entropy metal diborides: A new class of high-entropy materials and a new type of ultrahigh temperature ceramics, Scientific Reports 6, 37946 (2016).
- [7] C. Oses, C. Toher, and S. Curtarolo, High-entropy ceramics, Nature Reviews Materials 5, 295 (2020).
- [8] O. N. Senkov, J. M. Scott, S. V. Senkova, F. Meisenkothen, D. B. Miracle, and C. F. Woodward, Microstructure and elevated temperature properties of a refractory tanbhfzrti alloy, Journal of Materials Science 47, 4062 (2012).
- [9] K.-H. Cheng, C.-H. Lai, S.-J. Lin, and J.-W. Yeh, Structural and mechanical properties of multi-element (alcrmotatizr)nx coatings by reactive magnetron sputtering, Thin Solid Films 519, 3185 (2011).

- [10] A. Gali and E. George, Tensile properties of high- and medium-entropy alloys, Intermetallics 39, 74 (2013).
- [11] J. Chen, P. Niu, Y. Liu, Y. Lu, X. Wang, Y. Peng, and J. Liu, Effect of Zr content on microstructure and mechanical properties of AlCoCrFeNi high entropy alloy, Materials & Design 94, 39 (2016).
- [12] X. Xian, Z. Zhong, B. Zhang, K. Song, C. Chen, S. Wang, J. Cheng, and Y. Wu, A high-entropy $V_{35}T_{135}Fe_{15}Cr_{10}Zr_5$ alloy with excellent high-temperature strength, Materials & Design **121**, 229 (2017).
- [13] J. Li, Q. Fang, B. Liu, and Y. Liu, Transformation induced softening and plasticity in high entropy alloys, Acta Materialia 147, 35 (2018).
- [14] Y. Cai, G. Wang, Y. Ma, Z. Cao, and X. Meng, High hardness dual-phase high entropy alloy thin films produced by interface alloying, Scripta Materialia 162, 281 (2019).
- [15] P.-K. Huang, J.-W. Yeh, T.-T. Shun, and S.-K. Chen, Multi-principal-element alloys with improved oxidation and wear resistance for thermal spray coating, Advanced Engineering Materials 6, 74 (2004).
- [16] C.-Y. Hsu, J.-W. Yeh, S.-K. Chen, and T.-T. Shun, Wear resistance and high-temperature compression strength of FCC CuCoNiCrAl_{0.5}Fe alloy with boron addition, Metallurgical and Materials Transactions A 35, 1465 (2004).
- [17] M.-H. Chuang, M.-H. Tsai, W.-R. Wang, S.-J. Lin, and J.-W. Yeh, Microstructure and wear behavior of $\mathrm{Al_xCo_{1.5}CrFeNi_{1.5}Ti_y}$ high-entropy alloys, Acta Materialia **59**, 6308 (2011).
- [18] N. Kumar, M. Fusco, M. Komarasamy, R. Mishra, M. Bourham, and K. Murty, Understanding effect of 3.5 wt.% NaCl on the corrosion of Al_{0.1}CoCrFeNi highentropy alloy, Journal of Nuclear Materials 495, 154 (2017).
- [19] C. Briant, Refractory metals and alloys, in *Encyclopedia of Materials: Science and Technology*, edited by K. J. Buschow, R. W. Cahn, M. C. Flemings, B. Ilschner, E. J. Kramer, S. Mahajan, and P. Veyssire (Elsevier, Oxford, 2001) pp. 8088 8095.
- [20] O. Senkov, G. Wilks, D. Miracle, C. Chuang, and P. Liaw, Refractory high-entropy alloys, Intermetallics 18, 1758 (2010).
- [21] O. Senkov, G. Wilks, J. Scott, and D. Miracle, Mechanical properties of $Nb_{25}Mo_{25}Ta_{25}W_{25}$ and $V_{20}Nb_{20}Mo_{20}Ta_{20}W_{20}$ refractory high entropy alloys, Intermetallics 19, 698 (2011).
- [22] O. N. Senkov, D. Isheim, D. N. Seidman, and A. L. Pilchak, Development of a refractory high entropy superalloy, Entropy 18, 10.3390/e18030102 (2016).
- [23] J. Chen, X. Zhou, W. Wang, B. Liu, Y. Lv, W. Yang, D. Xu, and Y. Liu, A review on fundamental of high entropy alloys with promising hightemperature properties, Journal of Alloys and Compounds 760, 15 (2018).
- [24] P. Sarker, T. Harrington, C. Toher, C. Oses, M. Samiee, J.-P. Maria, D. W. Brenner, K. S. Vecchio, and S. Curtarolo, High-entropy high-hardness metal carbides discovered by entropy descriptors, Nature Communications 9, 4980 (2018).
- [25] A. Vazquez and S. Varma, High-temperature oxidation behavior of nbsicr alloys with hf additions, Journal of Alloys and Compounds 509, 7027 (2011).
- [26] B. Li, S. Jiang, and K. Zhang, Effects of w content on high temperature oxidation resistance and room tem-

- perature mechanical properties of hot-pressing Nb- χ W alloys, Materials Science and Engineering: A **556**, 15 (2012).
- [27] E. Castle, T. Csanádi, S. Grasso, J. Dusza, and M. Reece, Processing and properties of high-entropy ultra-high temperature carbides, Scientific Reports 8, 8609 (2018).
- [28] J. Dusza, P. vec, V. Girman, R. Sedlk, E. G. Castle, T. Csandi, A. Kovalkov, and M. J. Reece, Microstructure of (Hf-Ta-Zr-Nb)C high-entropy carbide at micro and nano/atomic level, Journal of the European Ceramic Society 38, 4303 (2018).
- [29] J.-W. Yeh, Alloy design strategies and future trends in high-entropy alloys, JOM 65, 1759 (2013).
- [30] R. Li, M. Li, C. Jiang, B. Qiao, W. Zhang, and J. Xu, Thermal stability of alcrtatizrmo-nitride high entropy film as a diffusion barrier for cu metallization, Journal of Alloys and Compounds 773, 482 (2019).
- [31] I. Choudhury and M. El-Baradie, Machinability of nickelbase super alloys: a general review, Journal of Materials Processing Technology 77, 278 (1998).
- [32] A. Pineau and S. D. Antolovich, High temperature fatigue of nickel-base superalloys a review with special emphasis on deformation modes and oxidation, Engineering Failure Analysis 16, 2668 (2009), special issue honouring Professor Manuel Elices on the occasion of his 70th birthday.
- [33] D. Miracle and O. Senkov, A critical review of high entropy alloys and related concepts, Acta Materialia 122, 448 (2017).
- [34] A. Baldereschi and K. Maschke, Band structure of semiconductor alloys beyond the virtual crystal approximation. effect of compositional disorder on the energy gaps in GaP_xAs_{I-x} , Solid State Communications **16**, 99 (1975).
- [35] W. Porod and D. K. Ferry, Modification of the virtualcrystal approximation for ternary iii-v compounds, Phys. Rev. B 27, 2587 (1983).
- [36] C. Maurizio, G. Mattei, P. Mazzoldi, S. Padovani, E. Cattaruzza, F. Gonella, F. DAcapito, and F. Zontone, Deviation from the virtual crystal approximation in disordered aucu alloy nanocrystals: Exafs and gixrd investigation, Nuclear Instruments and Methods in Physics Research Section B: Beam Interactions with Materials and Atoms 200, 178 (2003), proceedings of the E-MRS 2002 Symposium I on Synchrotron Radiation and Materials Science.
- [37] O. K. Orhan, M. Isiet, L. Caparini, and M. Ponga, Exploring the compositional space of high-entropy alloys for cost-effective high-temperature applications, Frontiers in Materials 8, 10.3389/fmats.2021.816610 (2022).
- [38] See Supplemental Materials URL, which includes Refs. [n-ml.
- [39] A. Fernndez-Caballero, M. Fedorov, J. S. Wrbel, P. M. Mummery, and D. Nguyen-Manh, Configurational entropy in multicomponent alloys: Matrix formulation from ab initio based hamiltonian and application to the fcc crfe-mn-ni system, Entropy 21, 10.3390/e21010068 (2019).
- [40] J. D. Eshelby and R. E. Peierls, The determination of the elastic field of an ellipsoidal inclusion, and related problems, Proceedings of the Royal Society of London. Series A. Mathematical and Physical Sciences 241, 376 (1957).
- [41] T. Mura, Isotropic inclusions, in *Micromechanics of defects in solids* (Springer Netherlands, Dordrecht, 1987) pp. 74–128.

- [42] G. Qin, R. Chen, H. Zheng, H. Fang, L. Wang, Y. Su, J. Guo, and H. Fu, Strengthening fcc-coerfemnni high entropy alloys by mo addition, Journal of Materials Science & Technology 35, 578 (2019).
- [43] D. F. Rojas, H. Li, O. K. Orhan, C. Shao, J. D. Hogan, and M. Ponga, Mechanical and microstructural properties of a CoCrFe_{0.75}NiMo_{0.3}Nb_{0.125} high-entropy alloy additively manufactured via cold-spray, Journal of Alloys and Compounds 893, 162309 (2022).
- [44] Q. Liu, X. Li, H. Liu, and Z. Guo, Multi-objective metaheuristics for discrete optimization problems: A review of the state-of-the-art, Applied Soft Computing 93, 106382 (2020).
- [45] M. Ashby, Multi-objective optimization in material design and selection, Acta Materialia 48, 359 (2000).
- [46] X. Fu, C. Schuh, and E. Olivetti, Materials selection considerations for high entropy alloys, Scripta Materialia 138, 145 (2017).
- [47] A. Gheribi, A. Pelton, E. Blisle, S. Le Digabel, and J.-P. Harvey, On the prediction of low-cost high entropy alloys using new thermodynamic multi-objective criteria, Acta Materialia 161, 73 (2018).
- [48] J. Kennedy and R. Eberhart, Particle swarm optimization, in *Proceedings of ICNN'95-international conference* on neural networks, Vol. 4 (IEEE, 1995) pp. 1942–1948.
- [49] M. Isiet and M. Gadala, Self-adapting control parameters in particle swarm optimization, Applied Soft Computing 83, 105653 (2019).
- [50] E. C. Laskari, K. E. Parsopoulos, and M. N. Vrahatis, Particle swarm optimization for integer programming, in Proceedings of the 2002 Congress on Evolutionary Computation. CEC'02 (Cat. No. 02TH8600), Vol. 2 (IEEE, 2002) pp. 1582–1587.
- [51] E. Houssein, A. Gad, K. Hussain, and P. N. Suganthan, Major advances in particle swarm optimization: theory, analysis, and application, Swarm and Evolutionary Computation 63, 100868 (2021).
- [52] S. Pervaiz, Z. Ul-Qayyum, W. H. Bangyal, L. Gao, and J. Ahmad, A systematic literature review on particle swarm optimization techniques for medical diseases detection, Computational and Mathematical Methods in Medicine 2021 (2021).
- [53] A. Thakkar and K. Chaudhari, A comprehensive survey on portfolio optimization, stock price and trend prediction using particle swarm optimization, Archives of Computational Methods in Engineering 28, 2133 (2021).
- [54] J. Jiao, S.-m. Ghoreishi, Z. Moradi, and K. Oslub, Coupled particle swarm optimization method with genetic algorithm for the static-dynamic performance of the magneto-electro-elastic nanosystem, Engineering with Computers , 1 (2021).
- [55] B. Steingrimsson, X. Fan, X. Yang, M. Gao, Y. Zhang, and P. K. Liaw, Predicting temperature-dependent ultimate strengths of body-centered-cubic (bcc) highentropy alloys, npj Computational Materials 7, 1 (2021).
- [56] O. K. Orhan, AFMDE: A Fair Materials Discovery Engine (2022).
- [57] P. Hohenberg and W. Kohn, Inhomogeneous electron gas, Phys. Rev. **136**, B864 (1964).
- [58] W. Kohn and L. J. Sham, Self-consistent equations in-

- cluding exchange and correlation effects, Phys. Rev. **140**, A1133 (1965).
- [59] J. P. Perdew, J. A. Chevary, S. H. Vosko, K. A. Jackson, M. R. Pederson, D. J. Singh, and C. Fiolhais, Atoms, molecules, solids, and surfaces: Applications of the generalized gradient approximation for exchange and correlation, Phys. Rev. B 46, 6671 (1992).
- [60] L. Nordheim, Zur elektronentheorie der metalle. i, Annalen der Physik 401, 607 (1900).
- [61] L. Bellaiche and D. Vanderbilt, Virtual crystal approximation revisited: Application to dielectric and piezoelectric properties of perovskites, Phys. Rev. B 61, 7877 (2000).
- [62] F. Tian, A review of solid-solution models of high-entropy alloys based on ab initio calculations, Frontiers in Materials 4, 36 (2017).
- [63] T. Li, J. W. Morris, N. Nagasako, S. Kuramoto, and D. C. Chrzan, "ideal" engineering alloys, Phys. Rev. Lett. 98, 105503 (2007).
- [64] L. Qi and D. C. Chrzan, Tuning ideal tensile strengths and intrinsic ductility of bcc refractory alloys, Phys. Rev. Lett. 112, 115503 (2014).
- [65] F. Tian, D. Wang, J. Shen, and Y. Wang, An ab initio investigation of ideal tensile and shear strength of tivnbmo high-entropy alloy, Materials Letters 166, 271 (2016).
- [66] Y. Mu, H. Liu, Y. Liu, X. Zhang, Y. Jiang, and T. Dong, An ab initio and experimental studies of the structure, mechanical parameters and state density on the refractory high-entropy alloy systems, Journal of Alloys and Compounds 714, 668 (2017).
- [67] R. G. Parr, R. A. Donnelly, M. Levy, and W. E. Palke, Electronegativity: The density functional viewpoint, The Journal of Chemical Physics 68, 3801 (1978).
- [68] X.-Q. Chen, H. Niu, D. Li, and Y. Li, Modeling hardness of polycrystalline materials and bulk metallic glasses, Intermetallics 19, 1275 (2011).
- [69] F. M. Gao and L. H. Gao, Microscopic models of hardness, Journal of Superhard Materials 32, 148 (2010).
- [70] M. Born and K. Huang, *Dynamical theory of crystal lattices*, Oxford classic texts in the physical sciences (Clarendon Press, Oxford, 1954).
- [71] H. Demarest, R. Ota, and O. Anderson, Prediction of high pressure phase transitions by elastic constant data, in *High-Pressure Research*, edited by M. H. Manghnani and S.-I. Akimoto (Academic Press, 1977) pp. 281–301.
- [72] S. P. Rudin, Generalization of soft phonon modes, Phys. Rev. B 97, 134114 (2018).
- [73] D. M. Teter, Computational alchemy: The search for new superhard materials, MRS Bulletin 23, 2227 (1998).
- [74] Y. Tian, B. Xu, and Z. Zhao, Microscopic theory of hardness and design of novel superhard crystals, International Journal of Refractory Metals and Hard Materials 33, 93 (2012).
- [75] S. Pugh, Relations between the elastic moduli and the plastic properties of polycrystalline pure metals, The London, Edinburgh, and Dublin Philosophical Magazine and Journal of Science 45, 823 (1954).
- [76] S. Boucetta, Theoretical study of elastic, mechanical and thermodynamic properties of mgrh intermetallic compound, Journal of Magnesium and Alloys 2, 59 (2014).

Supplemental Material

Short-ranged ordering for improved mean-field simulation of disordered media: insights from refractory-metal high-entropy alloy carbonitrides

Okan K. Orhan, ^{1,2} Mewael Isiet, ² Mauricio Ponga, ² and David D. O'Regan ¹ School of Physics, SFI AMBER Centre, and CRANN Institute,

Trinity College Dublin, the University of Dublin, Ireland

² Department of Mechanical Engineering, the University of British Columbia,

2054 - 6250 Applied Science Lane, Vancouver, BC, V6T 1Z4, Canada

Indexing the equi-molar random-solid solutions of the refractory-metals carbonitrides

In this work, the virtual-crystal approximation (VCA) [1, 2] is separately applied to the atoms, occupying the two sub-lattice sites of the B32 structure. The elemental pseudo-potentials of carbon (C) and nitrogen (N) are mixed with the equi-molar fractions to obtain the virtual atom Y², occupying the non-metallic sites. Similarly, the elemental pseudo-potentials of the six refractory metals are mixed into equi-molar compositions. For traceable notation, the refractory metals are denoted by X_i^1 , for which i = 1, ..., 6 representing zirconium (Zr), niobium (Nb), molybdenum (Mo), hafnium (Hf), tantalum (Ta), and tungsten (W), receptively. Following this notation, a virtual atom representing the equi-molar mixtures of the m refractory metals is denoted by X_i^m , for which the subscript i represents the ith combination, listed in Table S1.

$X_1^1 \to Zr$	$X_1^3 \to ZrNbMo$	$X_2^4 \rightarrow ZrNbMoTa$
$X_2^1 \to Nb$	$X_2^3 \to ZrNbHf$	$X_3^4 \rightarrow ZrNbMoW$
$X_3^1 \to Mo$	$X_3^3 \to ZrNbTa$	$X_4^4 \rightarrow ZrNbHfTa$
$X_4^1 \to Hf$	$X_4^3 \to ZrNbW$	$X_5^4 \rightarrow ZrNbHfW$
$X_5^1 \to Ta$	$X_5^3 \to ZrMoHf$	$X_6^4 \rightarrow ZrNbTaW$
$X_6^1 \to W$	$X_6^3 \to ZrMoTa$	$X_7^4 \rightarrow ZrMoHfTa$
$X_1^2 \to ZrNb$	$X_7^3 \to ZrMoW$	$X_8^4 \rightarrow ZrMoHfW$
$X_2^2 \to ZrMo$	$X_8^3 \to ZrHfTa$	$X_9^4 \to ZrMoTaW$
$\mathrm{X}_3^2 ightarrow \mathrm{ZrHf}$	$X_9^3 \to ZrHfW$	$X_{10}^4 o ZrHfTaW$
${ m X}_4^2 ightarrow { m ZrTa}$	$X_{10}^3 \to ZrTaW$	$X_{11}^4 o ext{NbMoHfTa}$
$X_5^2 o ZrW$	$X_{11}^3 \rightarrow \text{NbMoHf}$	$X_{12}^4 \rightarrow \text{NbMoHfW}$
$X_6^2 \to NbMo$	$X_{12}^3 \rightarrow \text{NbMoTa}$	$X_{13}^4 \rightarrow \text{NbMoTaW}$
$X_7^2 \to NbHf$	$X_{13}^3 \to \text{NbMoW}$	$X_{14}^4 \rightarrow \text{NbHfTaW}$
$X_8^2 o NbTa$	$X_{14}^3 \rightarrow \text{NbHfTa}$	$X_{15}^4 o ext{MoHfTaW}$
$X_9^2 \to NbW$	$X_{15}^3 \rightarrow \text{NbHfW}$	$X_1^5 o ZrNbMoHfTa$
$X_{10}^2 \to MoHf$	$X_{16}^3 \to \text{NbTaW}$	$X_2^5 \rightarrow ZrNbMoHfW$
$X_{11}^2 o MoTa$	$X_{17}^3 o MoHfTa$	$X_3^5 \rightarrow ZrNbMoTaW$
$X_{12}^2 \to \mathrm{MoW}$	$X_{18}^3 \rightarrow MoHfW$	$X_4^5 \rightarrow ZrNbHfTaW$
$\mathrm{X}^2_{13} ightarrow \mathrm{HfTa}$	$X_{19}^3 \to \text{MoTaW}$	$X_5^5 \rightarrow ZrMoHfTaW$
$X_{14}^2 \to HfW$	$X_{20}^3 \rightarrow HfTaW$	$X_6^5 o ext{NbMoHfTaW}$
$X_{15}^2 \rightarrow TaW$	$X_1^4 \to ZrNbMoHf$	$X_1^6 \to ZrNbMoHfTaW$

TABLE S1: Notation used to denote the random-solid solutions of the equi-molar refractory-metal alloys.

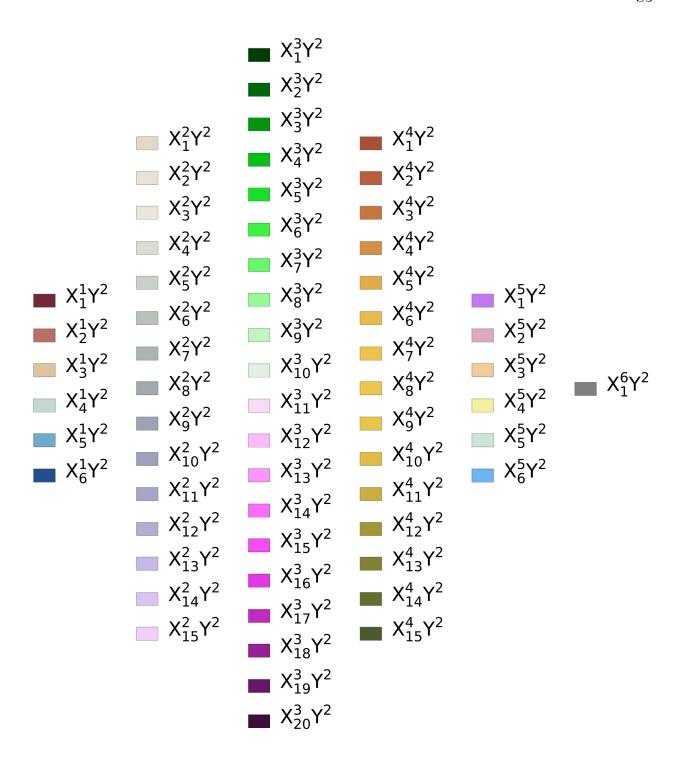


FIG. S1: Colors used to represent the random-solid solutions of the equi-molar refractory metal alloys in figures.

Approximate Gibbs free energy

For a non-magnetic solid, the Gibbs free energy (GFE) can be given by the sum

$$G = H + F_{\rm el} + F_{\rm vib} - TS_{\rm conf}, \tag{S1}$$

where T is the temperature. The formation enthalpy, H, can be simply taken as the groundstate energy at the equilibrium volume under no external potential such as $H = E_0$. The second term the electronic Helmholtz free energy, given by [3–5]

$$F_{\rm el} = \int_{-\infty}^{\infty} d\epsilon \ g(\epsilon) f - \int_{-\infty}^{E_{\rm F}} d\epsilon \ \epsilon g(\epsilon) + k_{\rm B} T \int_{-\infty}^{\infty} d\epsilon \ g(\epsilon) \left[f \ln(f) + (1 - f) \ln(1 - f) \right], \quad (S2)$$

where $k_{\rm B}$ and $E_{\rm F}$ are the Boltzmann constant and the Fermi energy, respectively; $f = f(\epsilon, T_{\rm e})$ and $g(\epsilon)$ are the Fermi-Dirac distribution function and the electronic density of states (DOS). The third term is the vibrational Helmholtz free energy, given by [6, 7]

$$F_{\rm vib} = k_{\rm B}T \int_0^\infty d\omega \ln \left[2 \sinh \left(\frac{\hbar \omega}{2k_{\rm B}T} \right) \right] p(\omega),$$
 (S3)

where $p(\omega)$ is the phonon DOS. The last term is due to the configuration entropy, S_{conf} , given within the Stirling approximation by [8]

$$S_{\text{conf}}(N) = -R \sum_{i}^{N} \alpha_{i} \ln(\alpha_{i}), \tag{S4}$$

where R and N are the gas constant and the number of principal elements, respectively, and α_i is the molar fraction of the i^{th} principal element. It is crucial to note that X_j^m and Y^2 exclusively occupy their respective sites; thus, Eq. (S5) becomes

$$S_{\text{conf}}(M) = R \left[ln(M) + ln(2) \right] \tag{S5}$$

for the equi-molar M-refractory-metals alloy carbonitrides.

Components of the mixing Gibbs free energy

Consistent with the components of the GFE in Eq. (S1), the components of the mixing GFE in Eq. (1) are given by

$$G_{\text{mix}} = H_{\text{mix}} + F_{\text{mix}}^{\text{el}} + F_{\text{mix}}^{\text{vib}} - TS_{\text{conf}}, \quad \text{where}$$

$$H_{\text{mix}} = H_{\text{MPEM}} - \sum_{i}^{N} \alpha_{i} H_{i},$$

$$F_{\text{mix}}^{\text{el}} = F_{\text{MPEM}}^{\text{el}} - \sum_{i}^{N} \alpha_{i} F_{i}^{\text{el}}, \quad \text{and} F_{\text{mix}}^{\text{vib}} = F_{\text{MPEM}}^{\text{vib}} - \sum_{i}^{N} \alpha_{i} F_{i}^{\text{vib}}.$$
(S6)

Mechanical stability assessment

The necessary and sufficient conditions for the elastic stability of cubic systems are within the Born-Huang stability criteria given by [9]

$$c_{11} - c_{12} > 0$$
, $c_{11} + 2c_{12} > 0$ and $c_{44} > 0$ (S7)

where c_{ij} are the elements of the second-order elastic tensor \mathbb{C} .

Mechanical properties and figures of merits

For the cubic symmetry, the Voigt- [10] and Reuss-averaged [11] bulk (K) and shear (S) modulus are given by [12]

$$K_{\rm V} = K_{\rm R} = \frac{C_{11} + 2c_{12}}{3},$$

$$S_{\rm V} = \frac{C_{11} - C_{12} + 3C_{44}}{5}, \text{ and } S_{\rm R} = \frac{5(C_{11} - C_{12})c_{44}}{3C_{11} - 3C_{12} + 4C_{44}},$$
(S8)

where C_{ij} is the entities of the second-order elastic tensor \mathbb{C} . The final Voigt-Reuss-Hill-averaged modulus [13] are simply $K = (K_{\rm V} + K_{\rm R})/2$ and $S = (S_{\rm V} + S_{\rm R})/2$. Using the VHR-averaged K and S, Young's modulus (Y) and the Poisson ratio $(\nu_{\rm P})$ are given by [14]

$$Y = \frac{9KS}{3K+S}$$
, and $\nu_{\rm P} = \frac{3K-2S}{6K+2S}$. (S9)

A critical minimum-value (CMV) of 0.25 for Poisson's ratio [15] commonly indicates large plastic deformation in solids. Moreover, the Pugh ratio, simply K/S, is used to assess ductility in solids with a CMV of 1.75 [16]. Finally, the Vickers hardness is commonly used as an industry-standard measure for wear resistance. It can be approximated using the semi-empirical relations, given by $H_{\rm V}^{\rm Teter} = 0.151S$ [17], or $H_{\rm V}^{\rm Tian} = 0.92(S/K)^{1.137}G^{0.708}$ [18]. The former one tends to underestimate, while the former one tends to overestimate. Thus, their average is used in this work such as $H_{\rm V} = 0.5(H_{\rm V}^{\rm Teter} + H_{\rm V}^{\rm Tian})$.

A. Computational details

The KS-DFT-based simulation were performed using the Quantum ESPRESSO (QE) software [19, 20], and its external routine, called the thermo_pw package [21], for thermodynamic simulations upto 1000 K. The SG15 optimized norm-conserving Vanderbilt (ONCV) scalar-relativistic pseudo-potentials [22, 23] using the Perdew-Burke-Ernzerhof (PBE) exchange-correlation functional [24–26] were used for the elemental atomic pseudo-potentials. An initial primitive unit cell of the B32 structure was used to generate the initial crystal structures. The electronic structure simulations were performed using a common kinetic energy cutoff of 150 Ry on a shifted $12 \times 12 \times 12$ Monkhorst-Pack-equivalent Brillouin zone sampling (MP-grid) [27] with a convergence for the total energies, a total forces, and a self-consistency were set to 10^{-7} Ry, 10^{-6} Ry· a_0^{-3} and 10^{-10} , respectively. The phonon dispersion simulations were performed on a $2 \times 2 \times 2$ MP-grid with a 10^{-10} self-consistency.

An in-house software was developed to calculate the short-ranged ordering (SRO) correction parameters using the unique adaptive particle-swarm optimization (UAPSO), and it is available at https://github.com/okorhan/AFMDE. A population size of 100 were used with a maximum iteration number of 5000 during UAPSO. As UAPSO is a stochastic approach, Each case was performed 10 times to ensure that the global optimum results were achieved.

Materials properties of the refractory-metals carbonitrides at the disordered mean-field limit

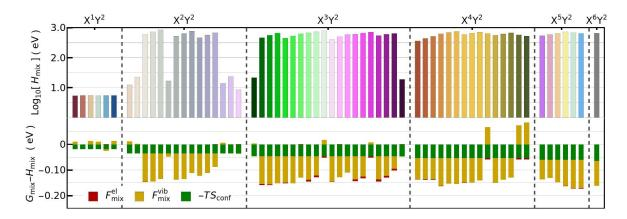


FIG. S2: Components of the mixing Gibbs free energy of the equi-molar refractory-metal carbonitrides at their mean-field disordered limit. The top panel shows the mixing enthalpy $(H_{\rm mix})$ in the logarithmic scale. The bottom panel shows the mixing electronic $(\Delta F_{\rm el})$, vibrational $(\Delta F_{\rm vib})$ Helmholtz free energies, and the configurational entropic contribution at $T=300~{\rm K}$.

X_1^1	1	1	1	X_1^3	1	1	✓	X_2^4	1	1	X
X_2^1	✓	✓	✓	X_2^3	X	✓	X	X_3^4	X	✓	X
X_3^1	✓	✓	✓	X_3^3	X	✓	X	X_4^4	✓	✓	✓
X_4^1	✓	✓	✓	X_4^3	✓	✓	✓	X_5^4	✓	✓	✓
X_5^1	✓	✓	✓	X_5^3	X	✓	X	X_6^4	✓	✓	✓
X_6^1	✓	✓	✓	X_6^3	✓	✓	✓	X_7^4	✓	✓	✓
X_1^2	✓	✓	✓	X_7^3	✓	✓	✓	X_8^4	✓	✓	✓
X_2^2	✓	✓	✓	X_8^3	X	✓	✓	X_9^4	✓	✓	✓
X_3^2	✓	✓	✓	X_9^3	✓	✓	X	X_{10}^{4}	✓	✓	✓
X_4^2	✓	✓	✓	X_{10}^{3}	✓	✓	✓	X_{11}^{4}	✓	✓	✓
X_5^2	✓	✓	✓	X_{11}^{3}	✓	✓	✓	X_{12}^{4}	✓	✓	✓
X_6^2	✓	✓	✓	X_{12}^{3}	✓	✓	✓	X_{13}^{4}	✓	✓	✓
X_7^2	✓	✓	✓	X_{13}^{3}	✓	✓	✓	X_{14}^{4}	✓	✓	✓
X_8^2	✓	✓	✓	X_{14}^{3}	X	✓	✓	X_{15}^{4}	✓	✓	✓
X_9^2	✓	✓	✓	X_{15}^{3}	✓	✓	X	X_1^5	✓	✓	✓
X_{10}^{2}	✓	✓	✓	X_{16}^{3}	✓	✓	✓	X_2^5	✓	✓	✓
X_{11}^{2}	✓	✓	✓	X_{17}^{3}	X	✓	✓	X_3^5	✓	✓	✓
X_{12}^2	✓	✓	✓	X_{18}^{3}	X	✓	✓	X_4^5	X	✓	✓
X_{13}^{2}	✓	✓	✓	X_{19}^{3}	✓	✓	X	X_5^5	X	✓	✓
X_{14}^{2}	✓	✓	✓	X_{20}^{3}	✓	✓	✓	X_6^5	X	✓	✓
X_{15}^{2}	✓	✓	✓	X_1^4	✓	✓	X	X_{1}^{6}	✓	✓	✓

TABLE S2: Elastic-stability assessment using the Born-Huang stability criteria for the cubic symmetry.

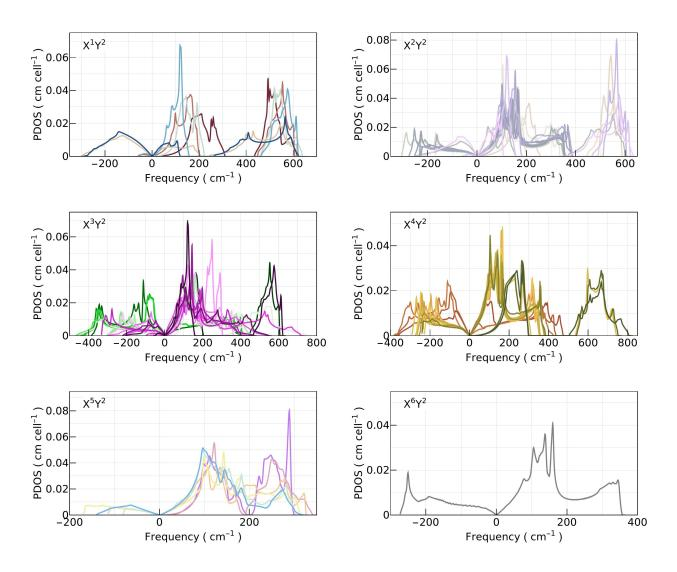


FIG. S3: Phonon density of states (PDOS) of the random-solid solutions of the equi-molar refractory-metal alloys.

		Expe		Calculate	ed	
	K	S	$H_{ m V}$	K	S	$H_{ m V}$
ZrC	207^{a}	172^{a}	$25.5^a, 25.8^b, 18.9^e$	225	162	23.90
NbC	296^{a}	214^a	$17.6^b, 19.65^a$	294	223	32.37
MoC	-	-	9.6^{c}	342	162	19.40
HfC	241^a	193^{a}	26.1^{a}	241	184	27.48
TaC	414^a	214^a	$16.7^a, 24.5^b$	316	234	33.23
WC	-	$262^{a,i}$	$22^{a,i}$	369	139	15.50
ZrN	215^{h}	160^{h}	$15.8^a, 13.3^e, 17.4^h$	248	148	19.96
NbN	292^{h}	165^{h}	$13.3^a, 20^h$	303	143	17.30
MoN	307^d	160^{d}	23^d	341	19	1.57
HfN	306^{h}	202^{h}	$16.3^a, 19.5^h$	263	155	20.71
TaN	-	-	$11^a, 22^b$	323	132	15.31
WN	-	-	29^e	365	-	-
-ZrY ²	-	-	24.8 ^e	243	176	25.65
-NbY ²	-	-	-	311	196	26.12
-MoY ²	-	-	14.61^{f}	351	114	12.26
$-$ HfY 2	-	-	32^g	258	191	27.94
$\overline{\text{TaY}^2}$	-	-	-	331	197	25.69
WY^2	-	-	-	376	58	5.31

TABLE S3: The calculated bulk (K) and shear (S) moduli, and Vickers hardness $(H_{\rm V})$ of the refractory-metal carbides, nitrites and carbonitrides alongside with available experimental values in literature.

 $[^]i$ Hexagonal structure

 $^{^{}a}{\rm Ref.~28,~^{b}Ref.~29,~^{c}Ref.~30,~^{d}Ref.~31,~^{e}Ref.~32,~^{f}Ref.~33,~^{g}Ref.~34,~^{h}Ref.~35}$

	$X_{1}^{5}Y^{2}$	$\mathrm{X}_{2}^{5}\mathrm{Y}^{2}$	$X_{3}^{5}Y^{2}$	$X_4^5Y^2$	$X_{5}^{5}Y^{2}$	$X_{6}^{5}Y^{2}$	$X_1^6Y^2$
K (GPa)	161	151	137	122	130	135	90
S (GPa)	32	37	28	-	-	-	30
$H_{ m V}$ (GPa)	3.29	4.04	2.93	-	-	-	3.76
$ u_{ m P}$	0.41	0.39	0.40	-	-	-	0.35
K/S	5.00	4.03	4.86	-	-	-	2.99

TABLE S4: The calculated bulk (K) and shear (S) moduli, Vickers hardness (H_V) , Poisson's ratio (ν_P) and the Pugh ratio (K/S) of the refractory-metal high-entropy alloy carbonitrides.

The short-ranged ordering correction parameters

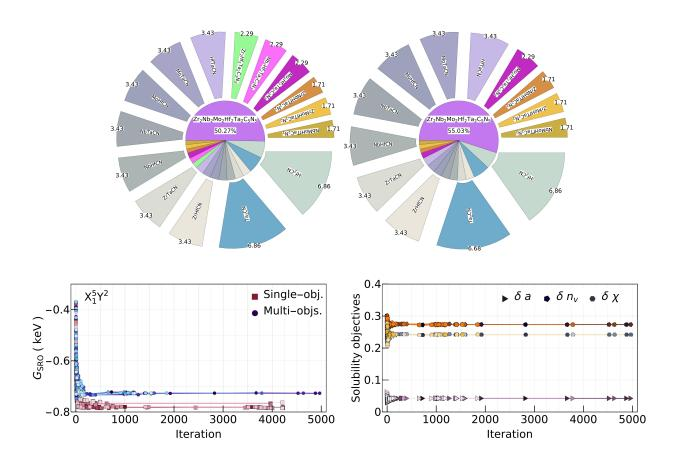


FIG. S4: The optimized short-ranged ordering correction parameters for $X_1^5Y^2$ and their convergences withing the unique adaptive particle-swarm optimization.

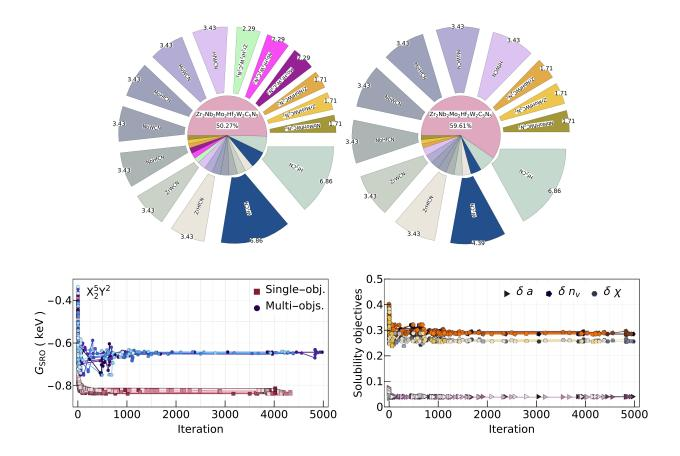


FIG. S5: The optimized short-ranged ordering correction parameters for $X_2^5Y^2$ and their convergences withing the unique adaptive particle-swarm optimization.

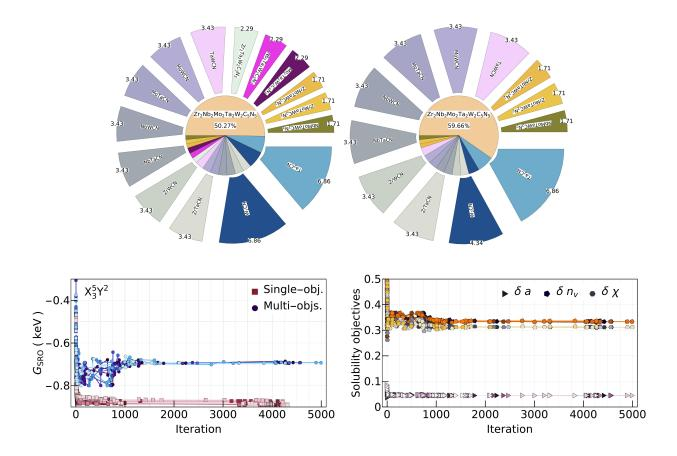


FIG. S6: The optimized short-ranged ordering correction parameters for $X_3^5Y^2$ and their convergences withing the unique adaptive particle-swarm optimization.

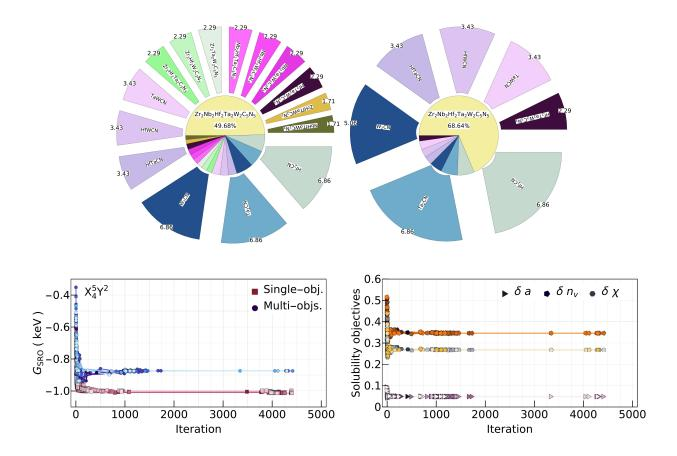


FIG. S7: The optimized short-ranged ordering correction parameters for $X_4^5Y^2$ and their convergences withing the unique adaptive particle-swarm optimization.

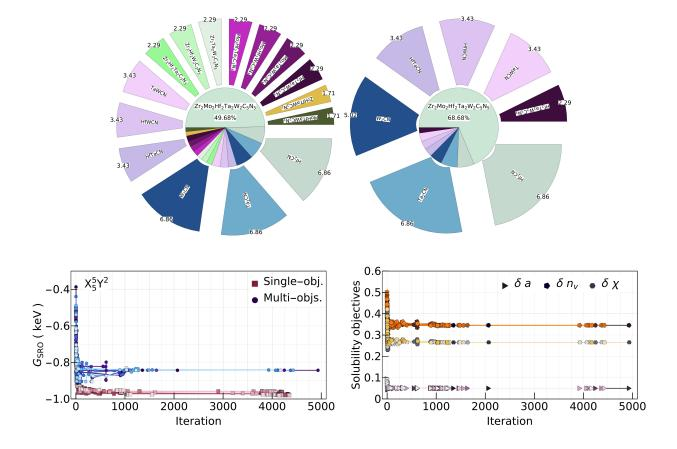


FIG. S8: The optimized short-ranged ordering correction parameters for $X_5^5Y^2$ and their convergences withing the unique adaptive particle-swarm optimization.

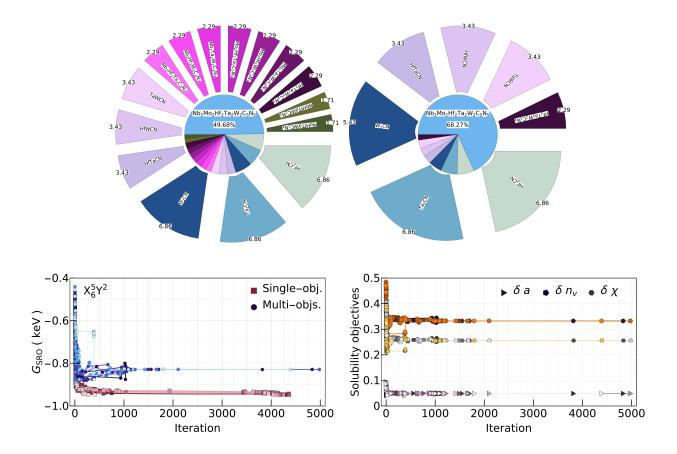


FIG. S9: The optimized short-ranged ordering correction parameters for $X_6^5Y^2$ and their convergences withing the unique adaptive particle-swarm optimization.

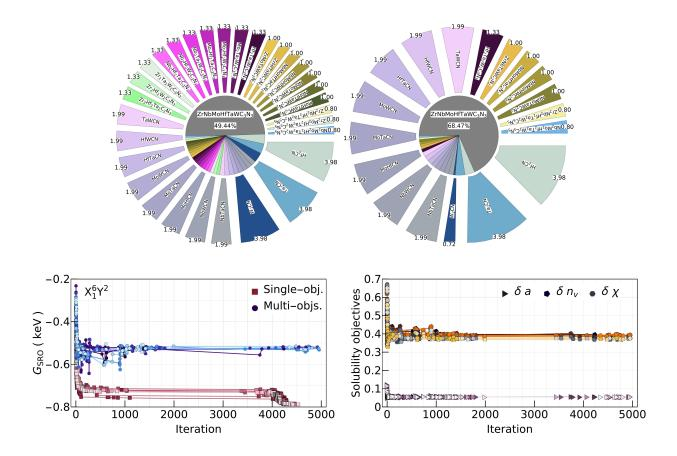


FIG. S10: The optimized short-ranged ordering correction parameters for $X_1^6Y^2$ and their convergences withing the unique adaptive particle-swarm optimization.

	$X_1^5 Y^2$	$X_{2}^{5}Y^{2}$	$X_3^5 Y^2$	$X_4^5Y^2$	$X_{5}^{5}Y^{2}$	$X_{6}^{5}Y^{2}$	$X_1^6Y^2$
$G_{ m mix}^{ m SRO}~({ m SO})$	-245.396	-243.584	-249.836	-305.790	-304.394	-309.478	-144.008
$G_{ m mix}^{ m SRO} \ ({ m MO})$	-185.961	-46.077	-45.697	-159.803	-161.625	-184.491	131.199

TABLE S5: The short-ranged ordering corrected mixing Gibbs free energy ($G_{\text{mix}}^{\text{SRO}}$ (in eV units) of the refractory-metal high-entropy alloy carbonitrides T=300 K using the single-objective (SO) and multi-objective (MO) optimized short-ranged ordering parameters (β_j^m).

- [2] L. Bellaiche and D. Vanderbilt, Virtual crystal approximation revisited: Application to dielectric and piezoelectric properties of perovskites, Phys. Rev. B **61**, 7877 (2000).
- [3] Y. Wang, Z.-K. Liu, and L.-Q. Chen, Thermodynamic properties of al, ni, nial, and ni3al from first-principles calculations, Acta Materialia **52**, 2665 (2004).
- [4] L. Landau and E. Lifshitz, Statistical physics (Pergamon Press, Headington Hill Hall, Oxford, OX3 0BW England, 1980) Chap. 5, pp. 158–168, 3rd ed.
- [5] F. Tian, A review of solid-solution models of high-entropy alloys based on ab initio calculations, Frontiers in Materials 4, 36 (2017).
- [6] A. van de Walle and G. Ceder, The effect of lattice vibrations on substitutional alloy thermodynamics, Rev. Mod. Phys. **74**, 11 (2002).
- [7] S.-L. Shang, Y. Wang, D. Kim, and Z.-K. Liu, First-principles thermodynamics from phonon and debye model: Application to ni and ni3al, Computational Materials Science 47, 1040 (2010).
- [8] L. J. Santodonato, Y. Zhang, M. Feygenson, C. M. Parish, M. C. Gao, R. J. K. Weber, J. C. Neuefeind, Z. Tang, and P. K. Liaw, Deviation from high-entropy configurations in the atomic distributions of a multi-principal-element alloy, Nature Communications 6, 5964 EP (2015), article.
- [9] F. Mouhat and F. m. c.-X. Coudert, Necessary and sufficient elastic stability conditions in various crystal systems, Phys. Rev. B 90, 224104 (2014).
- [10] W. den Voigt, Ueber die beziehung zwischen beiden elasticitätsconstanten isotroper körper, Annalen der Physik **274**, 573 (1889),https://onlinelibrary.wiley.com/doi/pdf/10.1002/andp.18892741206.
- [11] A. Reuss, Berechnung der fließgrenze von mischkristallen auf grund der plastizitätsbedingung für einkristalle ., ZAMM - Journal of Applied Mathematics and Mechanics / Zeitschrift für Angewandte Mathematik und Mechanik 9, 49 (1929).
- [12] P. Hao, P. Chen, L. Deng, F. Li, J. Yi, D. Şopu, J. Eckert, J. Tao, Y. Liu, and R. Bao, Anisotropic elastic and thermodynamic properties of the hcp-titanium and the fcc-titanium structure under different pressures, Journal of Materials Research and Technology 9, 3488 (2020).
- [13] R. Hill, The elastic behaviour of a crystalline aggregate, Proceedings of the Physical Society. Section A 65, 349 (1952).

- [14] A. Sarkar, L. Velasco, D. Wang, Q. Wang, G. Talasila, L. de Biasi, C. Kübel, T. Brezesinski, S. S. Bhattacharya, H. Hahn, and B. Breitung, High entropy oxides for reversible energy storage, Nature Communications 9, 3400 (2018).
- [15] S. Pugh, Relations between the elastic moduli and the plastic properties of polycrystalline pure metals, The London, Edinburgh, and Dublin Philosophical Magazine and Journal of Science 45, 823 (1954).
- [16] S. Boucetta, Theoretical study of elastic, mechanical and thermodynamic properties of mgrh intermetallic compound, Journal of Magnesium and Alloys 2, 59 (2014).
- [17] D. M. Teter, Computational alchemy: The search for new superhard materials, MRS Bulletin **23**, 22–27 (1998).
- [18] Y. Tian, B. Xu, and Z. Zhao, Microscopic theory of hardness and design of novel superhard crystals, International Journal of Refractory Metals and Hard Materials 33, 93 (2012).
- [19] P. Giannozzi, S. Baroni, N. Bonini, M. Calandra, R. Car, C. Cavazzoni, D. Ceresoli, G. L. Chiarotti, M. Cococcioni, I. Dabo, A. D. Corso, S. de Gironcoli, S. Fabris, G. Fratesi, R. Gebauer, U. Gerstmann, C. Gougoussis, A. Kokalj, M. Lazzeri, L. Martin-Samos, N. Marzari, F. Mauri, R. Mazzarello, S. Paolini, A. Pasquarello, L. Paulatto, C. Sbraccia, S. Scandolo, G. Sclauzero, A. P. Seitsonen, A. Smogunov, P. Umari, and R. M. Wentzcovitch, Quantum espresso: a modular and open-source software project for quantum simulations of materials, Journal of Physics: Condensed Matter 21, 395502 (2009).
- [20] P. Giannozzi, O. Andreussi, T. Brumme, O. Bunau, M. B. Nardelli, M. Calandra, R. Car, C. Cavazzoni, D. Ceresoli, M. Cococcioni, N. Colonna, I. Carnimeo, A. D. Corso, S. de Gironcoli, P. Delugas, R. A. D. Jr, A. Ferretti, A. Floris, G. Fratesi, G. Fugallo, R. Gebauer, U. Gerstmann, F. Giustino, T. Gorni, J. Jia, M. Kawamura, H.-Y. Ko, A. Kokalj, E. Küçükbenli, M. Lazzeri, M. Marsili, N. Marzari, F. Mauri, N. L. Nguyen, H.-V. Nguyen, A. O. de-la Roza, L. Paulatto, S. Poncé, D. Rocca, R. Sabatini, B. Santra, M. Schlipf, A. P. Seitsonen, A. Smogunov, I. Timrov, T. Thonhauser, P. Umari, N. Vast, X. Wu, and S. Baroni, Advanced capabilities for materials modelling with q uantum espresso, Journal of Physics: Condensed Matter 29, 465901 (2017).
- [21] Thermo_pw:Ab-initio computation of material properties, https://dalcorso.github.io/thermo_pw/, accessed: 18.09.2019.
- [22] D. R. Hamann, Optimized norm-conserving vanderbilt pseudopotentials, Phys. Rev. B 88,

- 085117 (2013).
- [23] M. Schlipf and F. Gygi, Optimization algorithm for the generation of once pseudopotentials, Computer Physics Communications **196**, 36 (2015).
- [24] D. R. Hamann, M. Schlüter, and C. Chiang, Norm-conserving pseudopotentials, Phys. Rev. Lett. 43, 1494 (1979).
- [25] G. P. Kerker, Non-singular atomic pseudopotentials for solid state applications, Journal of Physics C: Solid State Physics 13, L189 (1980).
- [26] D. R. Hamann, Generalized norm-conserving pseudopotentials, Phys. Rev. B 40, 2980 (1989).
- [27] H. J. Monkhorst and J. D. Pack, Special points for brillouin-zone integrations, Phys. Rev. B 13, 5188 (1976).
- [28] H. O. Pierson, Handbook of Refractory Carbides & Nitrides: Properties, Characteristics, Processing and Apps. (William Andrew, 1996).
- [29] X. Guo, L. Li, Z. Liu, D. Yu, J. He, R. Liu, B. Xu, Y. Tian, and H.-T. Wang, Hardness of covalent compounds: Roles of metallic component and d valence electrons, Journal of Applied Physics 104, 023503 (2008).
- [30] E. Saur, H. Schechinger, and L. Rinderer, Preparation and superconducting properties of mon and moc in form of wires, IEEE Transactions on Magnetics 17, 1029 (1981).
- [31] S. Wang, D. Antonio, X. Yu, J. Zhang, A. L. Cornelius, D. He, and Y. Zhao, The hardest superconducting metal nitride, Scientific Reports 5, 13733 (2015).
- [32] M. Larijani, M. Zanjanbar, and A. Majdabadi, The effect of carbon fraction in zr(c, n) films on the nano-structural properties and hardness, Journal of Alloys and Compounds 492, 735 (2010).
- [33] J. Kozłowski, J. Markowski, A. Prajzner, and J. Zdanowski, Properties of carbides, nitrides and carbonitrides based on ti and mo multicomponent layers, Surface and Coatings Technology 98, 1440 (1998), papers presented at the Fifth International Conference on Plasma Surface Engineering.
- [34] W. Piedrahita, W. Aperador, J. Caicedo, and P. Prieto, Evolution of physical properties in hafnium carbonitride thin films, Journal of Alloys and Compounds **690**, 485 (2017).
- [35] X.-J. Chen, V. V. Struzhkin, Z. Wu, M. Somayazulu, J. Qian, S. Kung, A. N. Christensen, Y. Zhao, R. E. Cohen, H.-k. Mao, and R. J. Hemley, Hard superconducting nitrides, Proceedings of the National Academy of Sciences 102, 3198 (2005).